Instantaneous GPS-Galileo Attitude Determination: Single-Frequency Performance in Satellite-Deprived Environments

Nandakumaran Nadarajah[1], Peter J. G. Teunissen[1,2], Noor Raziq[1]

***Abstract*—New and modernized Global Navigation Satellite Systems (GNSS) pave the way for an increasing number of applications in positioning, navigation, and timing (PNT). A combined GNSS constellation will significantly increase the number of visible satellites and thus will improve the geometry of observed satellites, enabling improvements in navigation solution availability, reliability, and accuracy. In this contribution a GPS+Galileo robustness analysis is carried out for instantaneous single-frequency GNSS attitude determination.**

Precise attitude determination using multiple GNSS antennas mounted on a platform relies on successful resolution of the integer carrier phase ambiguities. The Multivariate Constrained Least-squares AMBiguity Decorrelation Adjustment (MC-LAMBDA) method has been developed for resolving the integer ambiguities of the nonlinearly constrained GNSS attitude model that incorporates the known antenna geometry. In this contribution the method is used to analyse the attitude determination performance of a combined GPS+Galileo system. Special attention is thereby given to the GPS and Galileo Inter-System Biases (ISBs).

The attitude determination performance is evaluated using GPS/Galileo data sets from a hardware-in-the-loop experiment and two real data campaigns. In the hardware-in-the-loop experiment, a full GPS/Galileo constellation is simulated and performance analyses are carried out under various satellite deprived environments, such as urban canyon, open pit and other satellite outages. In the first real-data experiment, single-frequency GPS data combined with data of GIOVE-A/B (the two experimental Galileo satellites) are used to analyse the two constellation attitude solutions. In the second real-data experiment, we present the results based on single-frequency data from one of the Galileo IOV satellites (Galileo orbit validation satellites) combined with data of GIOVE-A and GPS. We demonstrate and quantify the improved availability, reliability, and accuracy of attitude determination using the combined constellation.

***Index Terms*—GNSS, GPS, Galileo, attitude determination, multivariate constrained integer least-squares, MC-LAMBDA, carrier phase ambiguity resolution, inter-system biases**

I. Introduction

Vehicular navigation using Global Navigation Satellite Systems (GNSS) has become ubiquitous. GNSS-only attitude (orientation) determination for land, airborne, and maritime vehicles has been explored using multiple GNSS receivers/antennas rigidly mounted on the platform [1]–[11]. The use of these methods under constrained (satellite deprived) environments such as urban canyon [12] and open-pit [13] is limited due to a lack of sufficient visible satellites. In light of new and modernized GNSS, however, the number of visible satellites will increase, thus resulting in an improved performance of positioning, navigation, and timing (PNT) solutions, in particular in constrained, satellite deprived environments, as well as offering operational back-up or independence in case of failure or unavailability of one system. Interoperability of the American GPS and the European Galileo system, currently under development, is important for assessing the PNT performance of the combined systems. At the time of analysis, the Galileo system consisted of two Galileo in-orbit validation element (GIOVE) satellites (GIOVE-A and -B launched in December 2005 and April 2008, respectively), and two in-orbit validation (IOV) satellites, namely Proto-flight model (PFM) and flight model (FM) co-launched in October 2011. The current contribution presents, for the first time, a combined GPS+Galileo attitude determination performance analysis. Its robustness is tested for different satellite-deprived environments with focus on the single-epoch, single-frequency case, as this is the most challenging scenario.

GNSS-based precise attitude determination relies on successful resolution of the integer carrier phase ambiguities. The Least squares AMBiguity Decorrelation Adjustment (LAMBDA) method [14] is currently the standard method for solving unconstrained and linearly constrained GNSS ambiguity resolution problems [15]–[20]. For such GNSS models, the method is known to be numerically efficient and optimal in the sense that it provides an integer ambiguity solution with the highest possible success-rate [21]–[23]. To exploit the known multi-antennae relative positions in local body frame, the multivariate constrained (MC-)LAMBDA method has been developed [24]–[30]. Due to the nonlinear antennae-geometry constraints, the search space of the integer carrier phase ambiguities is then no longer ellipsoidal, thus requiring special methods for the numerically efficient evaluation of the nonlinear multivariate ambiguity objective function [31], [32].

In this contribution we analyse the single-frequency, single-epoch GNSS attitude determination performance using combined GPS and Galileo observations. The analyses include a study of the performance robustness under various satellite-deprived environments, whereby also the antennae-geometry constrained performance is compared with the unconstrained

[1]GNSS Research Centre, Department of Spatial Sciences, Curtin University, Australia

[2]Delft Institute of Earth Observation and Space Systems (DEOS), Delft University of Technology, The Netherlands

Emails: n.nadarajah@curtin.edu.au, p.teunissen@curtin.edu.au, noor.raziq@curtin.edu.au

attitude determination performance. These studies are carried out using data sets from a hardware-in-the-loop experiment and two real data campaigns. In the hardware-in-the-loop experiment, a full GPS/Galileo constellation is simulated. For the real-data, two sets of data involving both constellations are used. Due to orbital parameters, co-visibility of Galileo experimental satellites does not exist for every day and hence, two unique periods were chosen: the first one having long GIOVE-A/-B co-visibility and the other one having long GIOVE-A/Galileo PFM co-visibility.

This contribution is organized as follows. Section II presents our attitude determination method for the combined GPS/Galileo constellation. We first describe the functional and stochastic model for combined GPS/Galileo observations, with special attention to inter-system biases and inter-system double-differencing. Then we describe the nonlinearly constrained GPS/Galileo attitude model and show how the solution of its multivariate ambiguity objective function is used to compute the ambiguity resolved attitude parameters. Section III presents the results of our performance analyses, first for the hardware-in-the-loop experiment and then for our real data experiments. We compare the instantaneous, single-frequency ambiguity resolution performance under various satellite-deprived environments, for GPS-only, Galileo-only and combined GPS/Galileo. This is done for the unconstrained (LAMBDA) as well as constrained (MC-LAMBDA) case. We also analyse both formal and empirical accuracies of the corresponding ambiguity resolved attitude parameters. Finally, Section IV contains the summary and conclusions of this contribution.

II. Attitude Determination for the Combined GPS-Galileo System

In this section we present our attitude determination method for the combined GPS-Galileo system. First we discuss different aspects of combined GPS-Galileo data processing and then we present the corresponding attitude model together with its multivariate constrained integer least-squares solution.

A. GPS/Galileo Observations

Attitude determination considered in this work is based on relative positioning using the so-called double differencing of GNSS observations. For combined GPS-Galileo observations, one can perform either system-specific double differencing [33] or inter-system double differencing [34], [35]. In the latter case, one should, however, take into account the inter-system bias (ISB) due to system specific hardware delays, more so when mixed receiver types are used. In this work, we use ISB corrected inter-system double differencing [36] which yields a higher level of redundancy than system-specific differencing.

Assuming that two GPS/Galileo receivers r and 1 collect pseudo-range and carrier-phase data on overlapping inter-system frequencies (L1-E1 and/or L5-E5A), the between-receiver single difference (SD) pseudo-range and carrier-phase observations at frequency j from GPS satellite s, denoted as p^s_{1r} and ϕ^s_{1r} respectively, are given as [37]

$$\mathrm{E}\left(p^s_{1r,j}\right) = \rho^s_{1r} + c\left[dt_{1r} + d^G_{1r,j}\right] + a^s_{1r,j} \quad (1)$$

$$\mathrm{E}\left(\phi^s_{1r,j}\right) = \rho^s_{1r} + c\left[dt_{1r} + \delta^G_{1r,j}\right] + \alpha^s_{1r,j} + \lambda_j M^s_{1r,j} \quad (2)$$

where $s = 1_G,\ \ldots,\ m_G$, $\mathrm{E}(\cdot)$ denotes expectation, ρ^s_{1r} is the SD topocentric distance, dt_{1r} is the SD receiver clock bias, $d^G_{1r,j}$ and $\delta^G_{1r,j}$ are the frequency- and system-dependent SD hardware biases inside the receiver, c is the speed of light, $a^s_{1r,j}$ and $\alpha^s_{1r,j}$ are the SD atmosphere delays, λ_j is the wave length, $M^s_{1r,j}$ is the time-invariant SD carrier-phase ambiguity, and m_G is the number of GPS satellites.

Similarly, the single difference Galileo observations are given as:

$$\mathrm{E}\left(p^q_{1r,j}\right) = \rho^q_{1r} + c\left[dt_{1r} + d^E_{1r,j}\right] + a^q_{1r,j} \quad (3)$$

$$\mathrm{E}\left(\phi^q_{1r,j}\right) = \rho^q_{1r} + c\left[dt_{1r} + \delta^E_{1r,j}\right] + \alpha^q_{1r,j} + \lambda_j M^q_{1r,j} \quad (4)$$

where $q = 1_E,\ \ldots,\ m_E$ and m_E is the number of Galileo satellites.

Inter-system double-differencing: In the case of double-differencing [36], we form double difference (DD) observables with respect to a GPS pivot satellite (or a Galileo pivot satellite) for both GPS and Galileo observations:

$$\mathrm{E}\left(p^{1_G s}_{1r,j}\right) = \rho^{1_G s}_{1r}, \qquad s = 2_G,\ \ldots,\ m_G \quad (5)$$

$$\mathrm{E}\left(\phi^{1_G s}_{1r,j}\right) = \rho^{1_G s}_{1r} + \lambda_j N^{1_G s}_{1r,j} \quad (6)$$

$$\mathrm{E}\left(p^{1_G q}_{1r,j}\right) = \rho^{1_G q}_{1r} + c d^{GE}_{1r,j}, \qquad q = 1_E,\ \ldots,\ m_E \quad (7)$$

$$\mathrm{E}\left(\phi^{1_G q}_{1r,j}\right) = \rho^{1_G q}_{1r} + c\delta^{GE}_{1r,j} + \lambda_j N^{1_G q}_{1r,j} \quad (8)$$

where 1_G is the GPS reference satellite, $(\cdot)^{1_G s}_{1r,j} = (\cdot)^s_{1r,j} - (\cdot)^{1_G}_{1r,j}$ denotes DD parameters, $N^{1_G s}_{1r,j} = M^s_{1r,j} - M^{1_G}_{1r,j}$ is the *integer* DD ambiguity, and $d^{GE}_{1r,j} = (d^E_{r,j} - d^E_{1,j}) - (d^G_{r,j} - d^G_{1,j})$ and $\delta^{GE}_{1r,j} = (\delta^E_{r,j} - \delta^E_{1,j}) - (\delta^G_{r,j} - \delta^G_{1,j})$ are the differential ISBs for code and phase observations, respectively.

Differential ISBs are shown to be constant and their values can be calibrated [36]. Hence, we may correct the Galileo observations a priori for the differential ISBs:

$$\mathrm{E}\left(p^{1_G q}_{1r,j} - c\tilde{d}^{GE}_{1r,j}\right) = \rho^{1_G q}_{1r}, \qquad q = 1_E,\ \ldots,\ m_E \quad (9)$$

$$\mathrm{E}\left(\phi^{1_G q}_{1r,j} - c\tilde{\delta}^{GE}_{1r,j}\right) = \rho^{1_G q}_{1r} + \lambda_j N^{1_G q}_{1r,j} \quad (10)$$

where $\tilde{d}^{GE}_{1r,j}$ and $\tilde{\delta}^{GE}_{1r,j}$ are the differential ISBs for code and phase known through calibration [36]. Note that, the ISBs are constant regardless of the receivers'/antennas' operating environment. Hence, ISBs can be computed based on static data set collected in a clean environment for one day with required accuracy (Table IX) and calibrated before using them for attitude determination of a moving vehicle. The redundancy of this model is equal to $2f[(m_G - 1) + m_E] - [3 + f(m_G - 1) + f m_E] = f(m_G + m_E - 1) - 3$ where f is the number of overlapping GPS-Galileo frequencies. For single frequency processing, which is considered in this paper, the redundancy is equal to $m_G + m_E - 4$. That is, the redundancy increases with m_E compared to a GPS only case ($m_E = 0$), implying that every additional Galileo satellite strengthens the

model.

From here on we consider the combined system (after ISB correction) as a single system with $m+1(=m_G+m_E)$ satellites. The linearized DD observation equations corresponding to (5), (6), (9), and (10) read

$$\begin{aligned} \mathrm{E}(\Delta p^{1s}_{1r,j}) &= {g_1^{1s}}^T b_r, \qquad s=2,\ \ldots,\ (m+1) \quad (11)\\ \mathrm{E}(\Delta \phi^{1s}_{1r,j}) &= {g_1^{1s}}^T b_r + \lambda_j N^{1s}_{1r,j} \quad (12)\end{aligned}$$

where $\Delta p^{1s}_{1r,j}$ and $\Delta \phi^{1s}_{1r,j}$ are the observed-minus-computed code and phase observations, b_r is the baseline vector containing relative position components, and g_1^{1s} is the geometry vector given as $g_1^{1s}=e_1^1-e_1^s$ with e_r^s the unit line-of-sight vector defined in Section III-B2. The vectorial forms of the DD observation equations for the rth baseline at the jth frequency read

$$\begin{aligned} \mathrm{E}(y_{p;r,j}) &= G_1 b_r \quad (13)\\ \mathrm{E}(y_{\phi;r,j}) &= G_1 b_r + \lambda_j z_{r,j} \quad (14)\end{aligned}$$

with $y_{p;r,j} = \left[\Delta p^{12}_{1r,j},\ \ldots,\ \Delta p^{1(m+1)}_{1r,j}\right]^T$, $y_{\phi;r,j} = \left[\Delta \phi^{12}_{1r,j},\ \ldots,\ \Delta \phi^{1(m+1)}_{1r,j}\right]^T$, $G_1 = \left[g_1^{12},\ \ldots,\ g_1^{1(m+1)}\right]^T$, $z_{r,j} = \left[N^{12}_{1r,j},\ \ldots,\ N^{1(m+1)}_{1r,j}\right]^T$.

For the stochastic modelling, we assume elevation dependent noise characteristics [38]. That is, the standard deviation of the undifferenced observable ς can be written as

$$\sigma_\varsigma(\epsilon) = \sigma_{\varsigma_0}\left(1+a_{\varsigma_0}\exp\left(\frac{-\epsilon}{\epsilon_{\varsigma_0}}\right)\right) \quad (15)$$

where ϵ is the elevation angle of the corresponding satellite, and σ_{ς_0}, a_{ς_0}, and ϵ_{ς_0} are the elevation dependent model parameters. We further assume that if the receivers/antennas have similar characteristics that the observation noise standard deviations can be decomposed as

$$\begin{aligned} \sigma_{\phi^s_{r,j}} &= \sigma_r \sigma_{,j} \sigma_{\phi_0} \nu^s\\ \sigma_{p^s_{r,j}} &= \sigma_r \sigma_{,j} \sigma_{p_0} \nu^s\\ \nu^s &= \left(1+a_0\exp\left(\tfrac{-\epsilon^s}{\epsilon_0}\right)\right)\end{aligned} \quad (16)$$

where σ_r and $\sigma_{,j}$ are the receiver and frequency dependent weightings, respectively, and σ_{ϕ_0} and σ_{p_0} are observation dependent weightings. Note that this assumption may not be valid in case of dissimilar receivers and/or antennas. In the real data analyses of Section III-B, such dissimilarity is taken into account by using different values for a_0 and/or ϵ_0.

B. GPS/Galileo Attitude Determination

This section describes the attitude determination for a small-sized array of GNSS receivers/antennas with known local body frame antenna geometry. First the multibaseline attitude model is introduced using the multivariate formulation of [25]. This formulation makes a frequent use of the Kronecker product $\otimes$ and the vec-operator [39], [40]. Then we include the local body frame antenna-geometry and show how the constrained attitude model can be solved in a step-wise manner.

1) The multivariate model: Let us consider a set of $r+1$ antennas rigidly mounted on a platform of interest and simultaneously tracking m_G GPS and m_E Galileo satellites on the same f frequencies (considered as a single system with $m+1=m_G+m_E$ satellites for inter-system double-differencing). Combining the linearized DD GNSS code and phase observations of (13) and (14) for the r baselines formed by these antennas, the single epoch *multivariate* observation model becomes:

$$\mathrm{E}(Y) = AZ+GB \qquad Z\in\mathbb{Z}^{fm\times r}, B\in\mathbb{R}^{3\times r} \quad (17)$$

where $Y=[y_1,\ldots,y_r]$ is the $2fm\times r$ matrix of r linearized (observed-minus-computed) DD observation vectors with $y_r=[y^T_{\phi;r}\ y^T_{p;r}]^T$, $y^T_{\phi;r}=[y^T_{\phi;r,1},\ldots,y^T_{\phi;r,f}]^T$, and $y^T_{p;r}=[y^T_{p;r,1},\ldots,y^T_{p;r,f}]^T$, $Z=[z_1,\ldots,z_r]$ is the $fm\times r$ matrix of r unknown DD integer ambiguity vectors $z_r=[z^T_{r,1},\ldots,z^T_{r,j}]^T$, $B=[b_1,\ldots,b_r]$ the $3\times r$ matrix of r unknown baseline vectors b_r, $G=e_{2f}\otimes G_1$ is the $2fm\times 3$ geometry matrix with e_{2f} the $2f\times 1$ vector of 1's, $A=L\otimes I_m$ is the $2fm\times fm$ design matrix with $2f\times f$ matrix $L=[\Lambda^T,\ 0^T]^T$ and $\Lambda=\mathrm{diag}(\lambda_1,\ldots,\lambda_f)$ the diagonal wavelength matrix. Note that, for the simplicity of the formulation, we assumed that all receivers/antennas track the same set of satellites. However, this restriction is relaxed in the software implemented using Matlab.

To construct the stochastic model for the multivariate array observations in (17), let us consider undifferenced observations in vector form reading

$$\zeta=[\zeta_1^T,\ \ldots,\ \zeta_{r+1}^T]^T \quad (18)$$

where $\zeta_r=[\phi_r^T\ p_r^T]^T$, $\phi_r=[\phi^T_{r,1},\ \ldots,\ \phi^T_{r,f}]^T$, $\phi_{r,j}=[\phi^1_{r,j},\ \ldots,\phi^{m+1}_{r,j}]^T$, $p_r=[p^T_{r,1},\ \ldots,\ p^T_{r,f}]^T$, $p_{r,j}=[p^1_{r,j},\ \ldots,p^{m+1}_{r,j}]^T$, and $p^s_{r,j}$ and $\phi^s_{r,j}$ are the undifferenced code and phase observations for $r-s$ receiver-satellite pair at jth frequency. With (16), assuming the observables to be normally distributed and mutually uncorrelated, the variance matrix (dispersion) of the observation vector ζ can be written as

$$\mathrm{D}(\zeta) = Q_r\otimes Q_f\otimes \mathrm{blockdiag}(Q_\phi,Q_p) \quad (19)$$

where $\mathrm{D}(\cdot)$ denotes the dispersion operator, $Q_r=\mathrm{diag}[\sigma_1^2,\ \ldots,\ \sigma^2_{r+1}]$, $Q_f=\mathrm{diag}[\sigma^2_{,1},\ \ldots,\ \sigma^2_{,f}]$, $Q_\phi=\sigma^2_{\phi_0}\mathrm{diag}[{\nu^1}^2,\ \ldots,\ {\nu^{m+1}}^2]$, and $Q_p=\sigma^2_{p_0}\mathrm{diag}[{\nu^1}^2\ \ldots\ {\nu^{m+1}}^2]$ are the co-factor matrices. The variance matrix of the DD observables is then given as

$$\mathrm{D}(\mathrm{vec}(Y))=\mathrm{D}(\mathcal{D}^T\zeta) \quad (20)$$

where the DD operator $\mathcal{D}^T$ is given as

$$\mathcal{D}^T=D_r^T\otimes I_f\otimes I_2\otimes D_m^T \quad (21)$$

with $D_n^T=[-e_n,\ I_n]$ the differencing matrix. Hence, the dispersion of the DD observables is given by the $2fmr\times 2fmr$ matrix

$$\mathrm{D}(\mathrm{vec}(Y)) = Q_{YY}=P\otimes Q_{yy} \quad (22)$$

where

$$P = D_r^T Q_r D_r \quad (23)$$
$$Q_{yy} = Q_f \otimes \text{blockdiag}(D_m^T Q_\phi D_m, D_m^T Q_p D_m) \quad (24)$$

The system of observation equations (17) forms together with the dispersion matrix (22) a *multivariate* Gauss-Markov model, with unknown integer matrix Z and unknown baseline matrix B. Once B has been determined, the platform attitude can be determined as well.

2) The body-frame antenna-geometry as multivariate constraints: The strength of the above model can be increased by including information about the geometry of the antenna configuration. The known body-frame antenna-geometry can be included into the above model through the parametrization

$$B = RB_0 \quad (25)$$

with the unknown $3 \times q$ orthogonal matrix R ($R^T R = I_q$) and the known $q \times r$ matrix B_0 describing the known geometry of the antenna configuration in the body frame. Here, q is the degree of geometrical independence of the GNSS baselines, for example, $q = 1$ for co-linearly installed antennas, $q = 2$ for co-planarly installed antennas, and $q = 3$ for antennas installed not in a single plane. For $q = 3$, R is related to the Euler attitude angles $\xi = [\phi\ \theta\ \psi]^T$ as follows:

$$R(\xi) = \begin{bmatrix} c_\theta c_\phi & -c_\psi s_\phi + s_\psi s_\theta c_\phi & s_\psi s_\phi + c_\psi s_\theta c_\phi \\ c_\theta s_\phi & c_\psi c_\phi + s_\psi s_\theta s_\phi & -s_\psi c_\phi + c_\psi s_\theta s_\phi \\ -s_\theta & s_\psi c_\theta & c_\psi c_\theta \end{bmatrix} \quad (26)$$

with ϕ the heading, θ the elevation, ψ the bank, and where $s_\alpha = \sin(\alpha)$ and $c_\alpha = \cos(\alpha)$. Note that for $q < 3$, only the first q columns of R are defined. For example, for a linear antenna array ($q = 1$) only the first column is defined and hence only heading and elevation are estimable.

Substitution of (25) into (17), leads to the constrained GNSS attitude model [31], [41]

$$\text{E}(Y) = AZ + GRB_0 \qquad Z \in \mathbb{Z}^{fm \times r} \quad (27)$$
$$\text{D}(\text{vec}(Y)) = Q_{YY} = P \otimes Q_{yy} \qquad R \in \mathbb{O}^{3 \times q} \quad (28)$$

Our objective is to solve for the attitude matrix R in a least-squares sense, thereby taking the integer constraints on matrix $Z \in \mathbb{Z}^{m \times r}$ and the orthonormality constraints on matrix $R \in \mathbb{O}^{3 \times q}$ into account. Hence, the least-squares minimization problem that will be solved reads

$$\min_{Z \in \mathbb{Z}^{fm \times r}, R \in \mathbb{O}^{3 \times q}} \|\text{vec}\,(Y - AZ - GRB_0)\|^2_{Q_{YY}} \quad (29)$$

with $||\cdot||^2_Q = (\cdot)^T Q^{-1} (\cdot)$. This is a mixed integer nonlinear least-squares problem that does not permit a closed-form solution. We now describe how (29) can be solved.

3) The real-valued float solution: The float solution is defined as the solution of (29) without the constraints. When we ignore the integer constraints on Z and the orthonormality constraints on R, the float solutions $\hat{Z}$ and $\hat{R}$, and their variance-covariance matrices are obtained from solving the system of normal equations:

$$\begin{bmatrix} Q_{\hat{z}\hat{z}} & Q_{\hat{z}\hat{R}} \\ Q_{\hat{R}\hat{z}} & Q_{\hat{R}\hat{R}} \end{bmatrix}^{-1} \cdot \begin{bmatrix} \text{vec}(\hat{Z}) \\ \text{vec}(\hat{R}) \end{bmatrix} = \begin{bmatrix} I_r \otimes A^T \\ B_0 \otimes G^T \end{bmatrix} Q_{YY}^{-1} \text{vec}(Y) \quad (30)$$

with

$$\begin{bmatrix} Q_{\hat{z}\hat{z}} & Q_{\hat{z}\hat{R}} \\ Q_{\hat{R}\hat{z}} & Q_{\hat{R}\hat{R}} \end{bmatrix} = \left(\begin{bmatrix} I_r \otimes A^T \\ B_0 \otimes G^T \end{bmatrix} Q_{YY}^{-1} \begin{bmatrix} I_s \otimes A & B_0^T \otimes G \end{bmatrix} \right)^{-1} \quad (31)$$

The Z-constrained solution of R and its variance-covariance matrix can be obtained from the float solution as follows

$$\text{vec}\left(\hat{R}(Z)\right) = \text{vec}(\hat{R}) - Q_{\hat{R}\hat{z}} Q_{\hat{z}\hat{z}}^{-1} \text{vec}\left(\hat{Z} - Z\right) \quad (32)$$
$$Q_{\hat{R}(Z)\hat{R}(Z)} = Q_{\hat{R}\hat{R}} - Q_{\hat{R}\hat{z}} Q_{\hat{z}\hat{z}}^{-1} Q_{\hat{z}\hat{R}} = \left(B_0 P^{-1} B_0^T\right)^{-1} \otimes \left(G^T Q_{yy}^{-1} G\right)^{-1} \quad (33)$$

Using the above estimators, the original problem in (29) can be decomposed as

$$\min_{Z \in \mathbb{Z}^{fm \times r}, R \in \mathbb{O}^{3 \times q}} \|\text{vec}\,(Y - AZ - GRB_0)\|^2_{Q_{YY}} = \left\|\text{vec}\left(\hat{E}\right)\right\|^2_{Q_{YY}} + \min_{Z \in \mathbb{Z}^{fm \times r}} \left(\left\|\text{vec}\left(\hat{Z} - Z\right)\right\|^2_{Q_{\hat{z}\hat{z}}} + \min_{R \in \mathbb{O}^{3 \times q}} \left\|\text{vec}\left(\hat{R}(Z) - R\right)\right\|^2_{Q_{\hat{R}(Z)\hat{R}(Z)}} \right) \quad (34)$$

with $\hat{E} = Y - A\hat{Z} - G\hat{R}B_0$ being the matrix of least-squares residuals. Note that the first term on the right hand side is constant, as it does not depend on the unknown matrices Z and R.

4) The integer ambiguity solution: Based on the orthogonal decomposition (34), the multivariate constrained integer minimization can be formulated as:

$$\check{Z} = \arg \min_{Z \in \mathbb{Z}^{fm \times r}} C(Z) \quad (35)$$

where

$$C(Z) = \left\|\text{vec}(\hat{Z} - Z)\right\|^2_{Q_{\hat{z}\hat{z}}} + \left\|\text{vec}\left(\hat{R}(Z) - \check{R}(Z)\right)\right\|^2_{Q_{\hat{R}(Z)\hat{R}(Z)}} \quad (36)$$

with

$$\check{R}(Z) = \arg \min_{R \in \mathbb{O}^{3 \times q}} \left\|\text{vec}\left(\hat{R}(Z) - R\right)\right\|^2_{Q_{\hat{R}(Z)\hat{R}(Z)}} \quad (37)$$

The ambiguity objective function $C(Z)$ is the sum of two coupled terms: the first weighs the distance from the float ambiguity matrix $\hat{Z}$ to the nearest integer matrix Z in the metric of $Q_{\hat{z}\hat{z}}$, while the second weighs the distance from the conditional float solution $\hat{R}(Z)$ to the nearest orthonormal matrix R in the metric of $Q_{\hat{R}(Z)\hat{R}(Z)}$.

Unlike with the standard LAMBDA method [14], the search space of the above integer minimization problem is non-ellipsoidal due to the presence of the second term in

$C(Z)$. This second term is a consequence of having the orthonormality constraints rigorously included. The evaluation of $C(Z)$ requires the computation of a nonlinear constrained least-squares problem (37) for every integer matrix in the search space. In the MC-LAMBDA method, this problem is mitigated through the use of easy-to-evaluate bounding functions [32]. Using these bounding functions, two strategies, namely the *Expansion* and the *Search and Shrink* strategies, were developed, see e.g. [24], [28]. These techniques avoid the computation of (37) for every integer matrix in the search space, and compute the integer minimizer $\check{Z}$ in an efficient manner.

5) The ambiguity resolved attitude solution: Finally, we obtain the integer ambiguity resolved attitude solution by substituting $\check{Z}$ into (32), thus giving $\hat{R}(\check{Z})$. The sought-for attitude angles $\xi\left(\check{Z}\right)$ are then obtained by solving the following nonlinear least squares problem:

$$\begin{aligned} \mathrm{E}\left(\hat{R}(\check{Z})\right) &= R(\xi) \\ \mathrm{D}\left(\mathrm{vec}\left(\hat{R}(\check{Z})\right)\right) &= Q_{\hat{R}(Z)\hat{R}(Z)} \end{aligned} \tag{38}$$

where $R(\xi)$ is defined in (26). Using a first order approximation, the formal variance-covariance matrix of the attitude angles is given by (see Appendix)

$$Q_{\xi\xi} \approx \left(J_{R,\xi}^T Q_{\hat{R}(Z)\hat{R}(Z)}^{-1} J_{R,\xi}\right)^{-1} \tag{39}$$

As the results in the next sections show, this first order approximation works well. This can be explained by the fact that once the ambiguities have been resolved, the precision of the attitude solution is driven by the high precision of the carrier phase observations.

III. Performance of GPS/Galileo Attitude Determination

In this section the performance analyses of GPS/Galileo attitude determination are presented. In the hardware-in-the-loop experiment (Section III-A), instantaneous, single-frequency attitude determination performance is studied for a full GPS/Galileo constellation under three different satellite-deprived environments, namely, satellite outage (Section III-A1), urban canyon (Section III-A2), and open-pit (Section III-A3), demonstrating the robustness of the MC-LAMBDA method in resolving integer ambiguities under these conditions compared to the standard LAMBDA method.

In the real data analyses (Section III-B), two sets of real data involving both constellations are considered. Due to orbital parameters, co-visibility of Galileo experimental satellites does not exist for every day and hence, two unique periods are chosen: the first one having long GIOVE-A/-B co-visibility (Section III-B1) and the other one having long GIOVE-A/Galileo PFM co-visibility (Section III-B2).

The performance measures considered for our analyses are linked to the two type of matrix parameters that need to be determined: the integer ambiguity matrix Z and the attitude matrix R. The GPS/Galileo attitude model's ability to correctly resolve Z is measured by the empirical instantaneous single-frequency ambiguity success fraction (relative frequency), defined as

$$\text{success fraction} = \frac{\text{number of correctly fixed epochs}}{\text{total number of epochs}} \tag{40}$$

where total number of epochs refer to the number time steps during the scenario considered regardless of whether ambiguities are fixed correctly or not. The single-frequency GPS/Galileo attitude model's ability to determine instantaneous attitude is measured by the ambiguity resolved angular accuracy, for which both the formal and empirical standard deviations are studied. Furthermore, the computational efficiency of the algorithm is measured by the average overall computation time based on Matlab implementation.

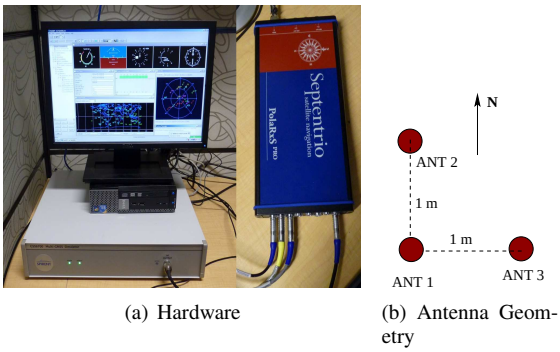

(a) Hardware (b) Antenna Geometry

Fig. 1. Hardware-in-the-loop simulation set up: a) Spirent GSS6700 multi-GNSS single-frequency simulator connected to Septentrio SEPT POLARXS receiver tracking GPS-Galileo L1-E1 signals b) simulated antenna geometry in the local body frame (forward-right-down with the origin at ANT1)

A. Hardware-in-the-loop Experiment

This section presents the analyses of full constellation data from a hardware-in-the-loop experiment to demonstrate the improved availability of GPS-Galileo based attitude determination. We used the Spirent GSS6700 multi-GNSS single-frequency simulator to generate GPS-Galileo L1-E1 signals, which were tracked by Septentrio PolaRxS$^{\mathrm{PRO}}$ receiver (Figure 1(a)). We considered a GPS constellation of 32 satellites and a Galileo constellation of 27 satellites to reflect the operational and the proposed missions, respectively. The simulated static platform is located at Perth, Australia (32° S 116° E) and equipped with three antennas forming a planar array as shown in Figure 1(b) for which the body frame coordinate matrix is given as

$$B_0 = \begin{bmatrix} 1 & 0 \\ 0 & 1 \end{bmatrix} \quad [\mathrm{m}] \tag{41}$$

The experiment was run for six hours with a start time of Dec 14, 2011 00:00:00 (UTC). After ignoring a few initial epochs due to cold-start of the receiver, we processed 20401 epochs of data at a rate of 1 Hz. Figure 2 shows the satellite visibility (the sky-plots, the number of satellites, and the PDOP values) during this period with an elevation cut-off angle of 10°. On average, the receiver tracked 10 GPS and 8 Galileo satellites reflecting satellite availabilities from prospective full constellations. Stochastic model parameters

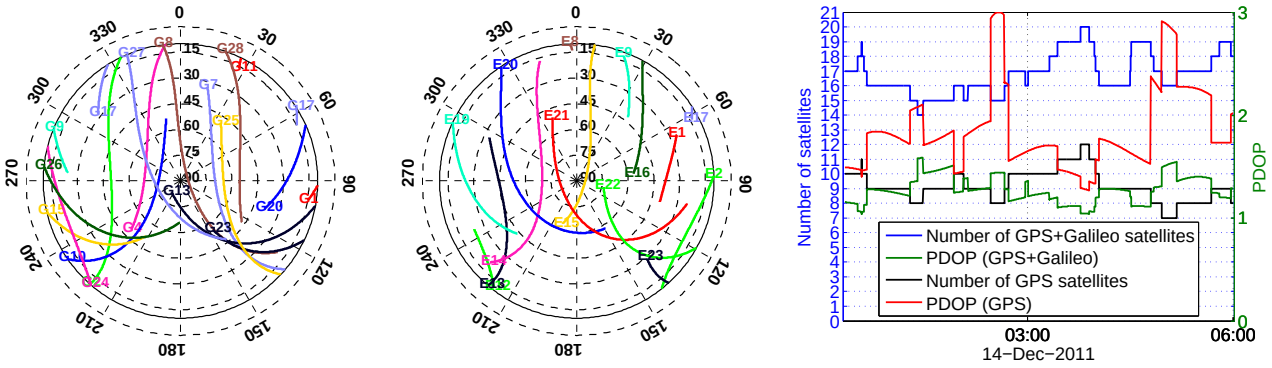

(a) Skyplot (GPS) (b) Skyplot (Galileo) (c) Number of satellites and PDOP

Fig. 2. Satellite visibility of GPS and Galileo constellations in the hardware-in-the-loop simulation with 10° elevation cut-off

System (Frequency)	Code σ_{p_0} [cm]	Code a_{p_0}	Code ϵ_{p_0} [deg]	Phase σ_{ϕ_0} [mm]	Phase a_{ϕ_0}	Phase ϵ_{ϕ_0} [deg]
GPS (L1)	30	0.3	20	1	0.3	20
Galileo (E1)	10	0.3	20	1	0.3	20

TABLE I
ELEVATION DEPENDENT STOCHASTIC MODEL PARAMETERS (15) FOR SEPTENTRIO RECEIVER USED IN THE HARDWARE-IN-THE-LOOP EXPERIMENT

for the elevation dependent model (15) of the receiver are reported in Table I. In the following sections, we discuss the results of single epoch, single-frequency (L1-E1) processing under various satellite deprived environments. We use the inter-system double differencing in all cases. Note that, ISBs are absent in this experiment as the same receiver was used to collect the observations from all three antennas.

1) Satellite Outage: Satellite outages are simulated by arbitrarily removing a number of visible satellites. Table II reports the formal and empirical angular accuracies as well as the ambiguity success fraction of the constrained MC-LAMBDA method (with Eq. 25) compared to that of the standard LAMBDA method (without Eq. 25). The cases with significant improvement are highlighted using bold text. Except for few severely deprived cases (with very few satellites), the MC-LAMBDA method is capable of resolving the correct ambiguities instantaneously with the success rate always better than (or equal to) standard LAMBDA method. Improved performance (robustness against satellite availability) of the MC-LAMBDA method compared to the standard LAMBDA method is due to the use of the geometry constraints. This, in turn, has increased computational complexity: as given in brackets the MC-LAMBDA has slightly high average overall computation time compared to that of the standard LAMBDA method.

The formal standard deviations (terms in brackets) are well in line with the empirical standard deviations confirming the assumed stochastic model parameters in Table I. Slight degradation of the angular accuracy with the number of satellites can be observed. Despite the slightly poor satellite geometry (slightly higher PDOP values) of the Galileo-only cases ($m_G = 0$), which leads to poor success rate performance compared to that of the GPS-only cases ($m_E = 0$), the angular estimation accuracy of Galileo-only processing is slightly better than that of GPS-only processing. This is due to the Galileo observables having a slightly higher signal-to-noise ratio (SNR) than that of GPS.

2) Urban Canyon: In this section we analyze the robustness of the MC-LAMBDA method under urban canyon effect, which is a well-known problem depriving GNSS based navigation solutions in urban environments [12], [42]–[44]. We simulate the blockage effect of urban canyon using a simple model, where we have two buildings as shown in Figure 3 placed symmetrically with respect to the attitude platform on an urban road. The blockage is defined by three angles: γ_0 the azimuth of the center of the first building (defining the direction of the road), α_0 the elevation at the center of the building (defining the height of the buildings), and β_0 the azimuth angle (defining the width of the buildings). For example, the severity of the blockage (for the case of $\gamma_0 = 90°$, $\alpha_0 = 60°$, and $\beta_0 = 60°$) becomes clear when Figure 4 is compared with the full visibility case of Figure 2. For these parameter values, the model represents two buildings with a height of 9 meters and a width of 17 meters on both sides of a ten-meter wide road in the North-South direction. Urban canyon can also introduce multi-path effect [12] and sometimes other types of interferences [45] that are not considered in this contribution. The robustness of the MC-LAMBDA method against multi-path effects has already been studied and demonstrated in [46] using a simulation study.

We considered the urban canyon along a road in North-South direction ($\gamma_0 = 90°$). This corresponds to the worst case deprivation due to a lack of visible satellites towards the South direction in Perth, Australia (South polar region). Table III summarizes the ambiguity resolution success fraction for the simulated urban canyon scenario demonstrating the robustness of the MC-LAMBDA method. Note that, for large values of α_0 and β_0, only a fraction of epochs (given in emphasized text) were processed due to the absence of sufficient satellites for positioning (requires at least four

m_G	m_E (PDOP)	Success fraction (computation time [sec]) LAMBDA	MC-LAMBDA	Angular standard deviation [deg] Heading	Elevation	Bank
0	4 (5.21)	0.00 (0.25)	0.58 (0.56)	0.07(0.08)	0.45 (0.49)	0.44 (0.49)
	6 (2.73)	0.47 (0.17)	**1.00** (0.20)	0.06(0.07)	0.24 (0.28)	0.24 (0.28)
	8 (2.13)	0.87 (0.18)	**1.00** (0.22)	0.05(0.06)	0.20 (0.23)	0.20 (0.23)
	10 (2.08)	0.89 (0.19)	**1.00** (0.22)	0.05(0.06)	0.19 (0.22)	0.19 (0.22)
2	4 (4.91)	0.29 (0.18)	0.99 (0.24)	0.07 (0.07)	0.31 (0.33)	0.30 (0.31)
	6 (2.45)	0.95 (0.19)	**1.00** (0.22)	0.06 (0.06)	0.23 (0.24)	0.22 (0.24)
	$\geq$ 8 (1.99)	1.00 (0.20)	1.00 (0.24)	0.05 (0.05)	0.19 (0.21)	0.19 (0.21)
4	0 (5.44)	0.00 (0.21)	0.22 (0.53)	0.13 (0.11)	0.58 (0.55)	0.53 (0.50)
	2 (3.69)	0.17 (0.20)	**1.00** (0.28)	0.09 (0.08)	0.28 (0.28)	0.27 (0.27)
	4 (2.35)	0.95 (0.18)	**1.00** (0.21)	0.06 (0.06)	0.21 (0.21)	0.21 (0.21)
	$\geq$ 6 (1.78)	1.00 (0.25)	1.00 (0.30)	0.05 (0.05)	0.18 (0.18)	0.18 (0.18)
6	0 (2.70)	0.11 (0.17)	**1.00** (0.21)	0.09 (0.08)	0.26 (0.23)	0.26 (0.24)
	2 (2.40)	0.93 (0.18)	**1.00** (0.21)	0.07 (0.06)	0.21 (0.20)	0.21 (0.20)
	4 (1.87)	0.99 (0.20)	**1.00** (0.23)	0.05 (0.05)	0.18 (0.18)	0.18 (0.18)
	$\geq$ 6 (1.49)	1.00 (0.28)	1.00 (0.32)	0.04 (0.04)	0.16 (0.16)	0.16 (0.16)
8	0 (2.04)	0.96 (0.18)	**1.00** (0.21)	0.07 (0.06)	0.22 (0.20)	0.22 (0.20)
	$\geq$ 2 (1.52)	1.00 (0.29)	1.00 (0.33)	0.05 (0.05)	0.15 (0.15)	0.15 (0.15)
10	0 (1.86)	0.99 (0.20)	**1.00** (0.23)	0.07 (0.06)	0.21 (0.19)	0.20 (0.18)
	$\geq$ 2 (1.44)	1.00 (0.35)	1.00 (0.39)	0.04 (0.04)	0.15 (0.15)	0.15 (0.15)
12	0 (1.85)	0.99 (0.19)	**1.00** (0.23)	0.07 (0.09)	0.21 (0.20)	0.20 (0.20)
	$\geq$ 2 (1.43)	1.00 (0.34)	1.00 (0.37)	0.04 (0.04)	0.15 (0.15)	0.15 (0.15)

TABLE II

INSTANTANEOUS SINGLE-FREQUENCY AMBIGUITY SUCCESS FRACTIONS (RELATIVE FREQUENCIES), THE AVERAGE COMPUTATION TIME [SEC] (GIVEN IN BRACKETS), AND EMPIRICAL AND FORMAL (GIVEN IN BRACKETS) ANGULAR STANDARD DEVIATIONS (BASED ON CORRECTLY FIXED EPOCHS) FOR THE HARDWARE-IN-THE-LOOP EXPERIMENT WITH SIMULATED SATELLITE OUTAGE (HERE, '$\geq s$' REFERS TO s OR MORE SATELLITES)

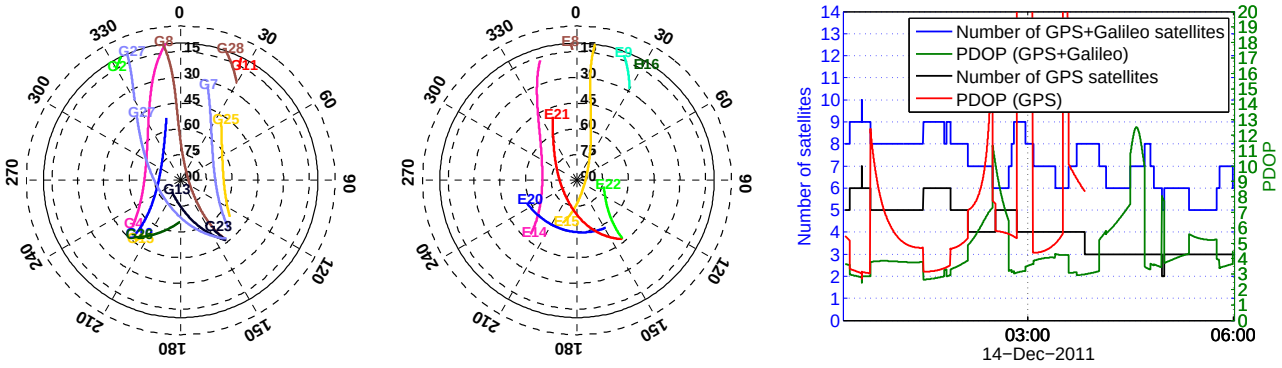

(a) Skyplot (GPS) (b) Skyplot (Galileo) (c) Number of satellites and PDOP

Fig. 4. Satellite visibility for simulated urban canyon with $\alpha_0 = 60°$ and $\beta_0 = 60°$ in the North-South direction

α_0 (deg)	β_0 (deg)	GPS only LAMBDA	MC-LAMBDA	Galileo only LAMBDA	MC-LAMBDA	GPS + Galileo LAMBDA	MC-LAMBDA
20	20	0.89 (0.14)	1.00 (0.18)	0.85 (0.13)	1.00 (0.16)	**1.00** (0.42)	1.00 (0.48)
	40	0.85 (0.16)	1.00 (0.20)	0.79 (0.13)	1.00 (0.17)	**1.00** (0.44)	1.00 (0.48)
	60	0.85 (0.15)	1.00 (0.18)	0.77 (0.13)	1.00 (0.17)	**1.00** (0.46)	1.00 (0.47)
	80	0.85 (0.18)	1.00 (0.19)	0.77 (0.16)	1.00 (0.20)	**1.00** (0.45)	1.00 (0.55)
40	20	0.86 (0.14)	1.00 (0.18)	0.78 (0.12)	1.00 (0.16)	**1.00** (0.37)	1.00 (0.41)
	40	0.68 (0.14)	1.00 (0.19)	0.55 (0.13)	1.00 (0.18)	**1.00** (0.32)	1.00 (0.36)
	60	0.37 (0.14)	0.97 (0.21)	0.15 (0.13)/*0.90*	0.97 (0.22)/*0.90*	**1.00** (0.24)	**1.00** (0.28)
	80	0.28 (0.13)	0.97 (0.22)	0.10 (0.12)/*0.90*	0.97 (0.22)/*0.90*	**1.00** (0.25)	**1.00** (0.29)
60	20	0.81 (0.14)	1.00 (0.18)	0.65 (0.13)	1.00 (0.17)	**1.00** (0.33)	1.00 (0.39)
	40	0.45 (0.15)	0.96 (0.21)	0.24 (0.13)/*0.99*	0.84 (0.28)/*0.99*	**1.00** (0.23)	**1.00** (0.27)
	60	0.03 (0.21)/*0.57*	0.77 (0.40)/*0.57*	$*$ $(*)$/*0.16*	$*$ $(*)$/*0.16*	0.75 (0.18)	**1.00** (0.22)
	80	0.01 (0.27)/*0.49*	0.69 (0.49)/*0.49*	$*$ $(*)$/*0.07*	$*$ $(*)$/*0.07*	0.71 (0.22)/*0.82*	1.00 (0.26)/*0.82*
80	20	0.71 (0.15)	1.00 (0.20)	0.59 (0.13)	0.98 (0.19)	**1.00** (0.30)	**1.00** (0.35)
	40	0.23 (0.14)/*0.92*	0.84 (0.30)/*0.92*	0.16 (0.13)/*0.85*	0.81 (0.28)/*0.85*	**1.00** (0.21)	**1.00** (0.25)
	60	$*$ $(*)$/*0.00*	$*$ $(*)$/*0.00*	$*$ $(*)$/*0.02*	$*$ $(*)$/*0.02*	0.06 (0.50)/*0.36*	0.99 (0.57)/*0.36*
	80	$*$ $(*)$/*0.00*	$*$ $(*)$/*0.00*	$*$ $(*)$/*0.00*	$*$ $(*)$/*0.00*	$*$ $(*)$/*0.00*	$*$ $(*)$/*0.00*

TABLE III

INSTANTANEOUS SINGLE-FREQUENCY AMBIGUITY SUCCESS FRACTIONS (RELATIVE FREQUENCIES) AND THE AVERAGE COMPUTATION TIME [SEC] (GIVEN IN BRACKETS) FOR THE HARDWARE-IN-THE-LOOP EXPERIMENT WITH SIMULATED URBAN CANYON (FIGURE 3); FOR SOME CASES, ONLY A FRACTION OF EPOCHS (GIVEN IN EMPHASIZED TEXT) WERE PROCESSED DUE TO A LACK OF SUFFICIENT SATELLITES FOR POSITIONING (REQUIRES AT LEAST FOUR SATELLITES)

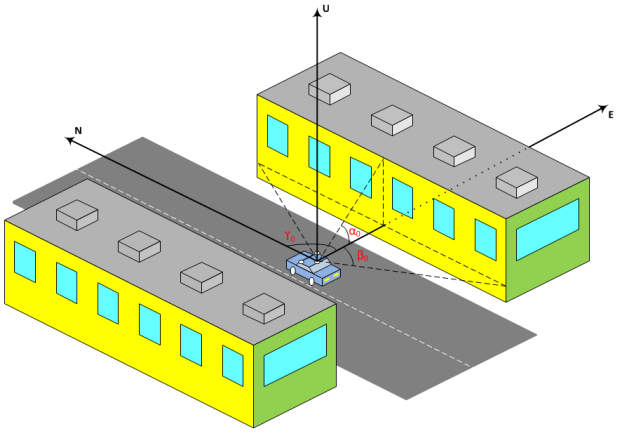

Fig. 3. Simulated urban canyon: Buildings on both sides of an urban road block satellite visibility; Angle γ_0 defines the direction of the road, while angles α_0 and β_0 define the height and the width of the buildings, respectively.

satellites). For almost all other cases, instantaneous ambiguity resolution is possible due to the exploitation of the geometry constraints in the MC-LAMBDA method, which requires slight high computational effort (given in brackets). The corresponding angular accuracies (standard deviations) are reported in Table IV, showing that empirical values are in line with formal values (given in brackets). Similar to the satellite outage problem of Section III-A1, the GPS-only success fraction is slightly better than that of the Galileo-only case due to better satellite geometry (small PDOP values, which are not given in the table). Also, similar to the satellite outage problem considered above, the Galileo-only angular accuracies are slightly better than that of the GPS-only cases due to the Galileo observables having slightly higher SNR than that of GPS. Both success fraction and angular accuracy degrade as the effect of the urban canyon increases (i.e., angles α_0 and β_0 increase). Except for the worst case scenario (i.e. $\alpha_0 = 80°$ and $\beta_0 = 80°$), the bold-texted results of Table III show that the MC-LAMBDA based, combined GPS-Galileo attitude solution is available with high ambiguity success fraction. A combined GPS/Galileo system processing not only improves the success fraction, but also slightly improves the angular accuracies (Table IV). Both the ambiguity resolution success fraction and the angular accuracy, however, degrade as the effect of the urban canyon increases (i.e., angles α_0 and β_0 increase).

3) Open-pit: In this section, the impact of an open-pit environment is analyzed. As shown in Figure 5 the platform is assumed to be at the center of an open-pit base. Tables V and VI report the ambiguity success fractions and the angular accuracies for the simulated open-pits, thus clearly highlighting the benefit of using a combined system and improved robustness of the MC-LAMBDA method with slightly increased computational load (given in brackets). That is, the MC-LAMBDA processing of a combined GPS/Galileo system enables the availability of instantaneous attitude solutions for an open-pit with up to 40 deg elevation masking.

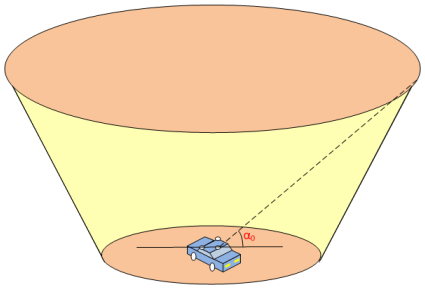

Fig. 5. Simulated circular open-pit; the elevation masking angle α_o defines the blockage. The platform is assumed to be at the center of open-pit base

(a) Antenna setup (b) Antenna geometry

Fig. 6. Curtin GNSS antennas used for the real data campaign

B. Real Data Campaign

The real data sets used for the analyses in this work are from three antennas mounted on the roof of building 402 at the campus of Curtin University in Perth, Australia. As shown in Figure 6(a), the antennas form a planar array as shown in Figure 6(b) for which the body frame coordinate matrix is given as

$$B_0 = \begin{bmatrix} 8.418 & -0.024 \\ 0 & 4.269 \end{bmatrix} \text{ [m]} \qquad (42)$$

These antennas are connected to three GNSS receivers whose connectivities are summarized in Table VII. All three receivers continuously track almost all available GNSS satellites.

The stochastic model parameters of the elevation dependent model (15) for the receivers are reported in Table VIII, indicating the different values for a_{p_0} and a_{ϕ_0}. In the following analyses, we use inter-system double differencing after correcting GNSS observations for the differential ISBs given in Table IX.

1) GPS/GIOVE Data: In this section, we present the results of attitude determination for the antennas shown in Figure

Antenna/Receiver	Antenna type	Receiver type
CUT0 & CUTA	TRM59800.00 SCIS	TRIMBLE NETR9
CUBB	JAV_GRANT-G3T	QUA_G3D_3

TABLE VII
CURTIN GNSS RECEIVER-ANTENNA CONNECTIVITY

α_0 (deg)	β_0 (deg)	GPS only Heading	GPS only Elevation	GPS only Bank	Galileo only Heading	Galileo only Elevation	Galileo only Bank	GPS + Galileo Heading	GPS + Galileo Elevation	GPS + Galileo Bank
20	20	0.07 (0.07)	0.24 (0.24)	0.24 (0.25)	0.06 (0.06)	0.20 (0.21)	0.20 (0.21)	0.04 (0.04)	0.14 (0.14)	0.14 (0.14)
	40	0.07 (0.07)	0.26 (0.26)	0.26 (0.27)	0.06 (0.06)	0.22 (0.22)	0.22 (0.22)	0.04 (0.04)	0.15 (0.15)	0.15 (0.15)
	60	0.07 (0.07)	0.27 (0.27)	0.27 (0.27)	0.06 (0.06)	0.23 (0.23)	0.23 (0.23)	0.04 (0.04)	0.15 (0.16)	0.15 (0.16)
	80	0.07 (0.07)	0.27 (0.27)	0.27 (0.27)	0.06 (0.06)	0.23 (0.23)	0.23 (0.23)	0.04 (0.04)	0.15 (0.16)	0.15 (0.16)
40	20	0.07 (0.07)	0.25 (0.25)	0.25 (0.25)	0.06 (0.06)	0.21 (0.22)	0.21 (0.22)	0.04 (0.04)	0.14 (0.15)	0.14 (0.15)
	40	0.08 (0.08)	0.37 (0.36)	0.37 (0.37)	0.06 (0.06)	0.25 (0.25)	0.25 (0.25)	0.05 (0.05)	0.16 (0.17)	0.16 (0.17)
	60	0.10 (0.10)	0.47 (0.46)	0.48 (0.48)	0.09 (0.09)	0.40 (0.41)	0.44 (0.45)	0.06 (0.06)	0.22 (0.22)	0.23 (0.24)
	80	0.10 (0.10)	0.51 (0.50)	0.52 (0.51)	0.09 (0.09)	0.42 (0.44)	0.47 (0.48)	0.06 (0.06)	0.25 (0.25)	0.26 (0.26)
60	20	0.08 (0.08)	0.25 (0.25)	0.25 (0.26)	0.06 (0.06)	0.21 (0.22)	0.22 (0.22)	0.04 (0.04)	0.14 (0.15)	0.14 (0.15)
	40	0.10 (0.10)	0.34 (0.33)	0.34 (0.34)	0.08 (0.08)	0.24 (0.25)	0.26 (0.26)	0.05 (0.05)	0.16 (0.17)	0.17 (0.17)
	60	0.15 (0.15)	0.42 (0.42)	0.46 (0.47)	0.15 (0.15)	0.34 (0.34)	0.42 (0.42)	0.11 (0.11)	0.29 (0.30)	0.36 (0.36)
	80	0.13 (0.13)	0.57 (0.57)	0.61 (0.62)	0.12 (0.12)	0.41 (0.41)	0.47 (0.46)	0.11 (0.11)	0.42 (0.44)	0.47 (0.49)
80	20	0.08 (0.08)	0.26 (0.27)	0.27 (0.27)	0.06 (0.06)	0.22 (0.22)	0.22 (0.23)	0.04 (0.04)	0.15 (0.15)	0.15 (0.15)
	40	0.09 (0.09)	0.36 (0.35)	0.37 (0.36)	0.07 (0.07)	0.23 (0.23)	0.24 (0.24)	0.05 (0.05)	0.18 (0.18)	0.18 (0.19)
	60	$*$ ($*$)	$*$ ($*$)	$*$ ($*$)	$*$ ($*$)	$*$ ($*$)	$*$ ($*$)	0.14 (0.14)	0.26 (0.27)	0.38 (0.38)
	80	$*$ ($*$)	$*$ ($*$)	$*$ ($*$)	$*$ ($*$)	$*$ ($*$)	$*$ ($*$)	$*$ ($*$)	$*$ ($*$)	$*$ ($*$)

TABLE IV
EMPIRICAL AND FORMAL (GIVEN IN BRACKETS) ANGULAR STANDARD DEVIATIONS [DEG] FOR HARDWARE-IN-THE-LOOP EXPERIMENT WITH SIMULATED URBAN CANYON (FIGURE 3)

Elevation Cut-off [deg]	GPS only LAMBDA	GPS only MC-LAMBDA	Galileo only LAMBDA	Galileo only MC-LAMBDA	GPS + Galileo LAMBDA	GPS + Galileo MC-LAMBDA
10	0.98 (0.16)	1.00 (0.19)	0.89 (0.13)	1.00 (0.16)	**1.00** (0.44)	1.00 (0.53)
20	0.70 (0.13)	1.00 (0.16)	0.58 (0.12)	1.00 (0.15)	**1.00** (0.31)	1.00 (0.35)
30	0.17 (0.13)	0.99 (0.20)	0.13 (0.12)/*0.94*	0.95 (0.21)/*0.94*	**1.00** (0.22)	1.00 (0.25)
40	0.03 (0.15)/*0.74*	0.81 (0.36)/*0.74*	0.00 (0.16)/*0.42*	0.82 (0.36)/*0.42*	0.87 (0.17)	**1.00** (0.21)
50	0.00 (0.39)/*0.14*	0.52 (0.64)/*0.14*	0.00 (0.80)/*0.09*	0.88 (1.00)/*0.09*	0.46 (0.22)/*0.68*	1.00 (0.26)/*0.68*
60	$*$ ($*$)/*0.00*	$*$ ($*$)/*0.00*	$*$ ($*$)/*0.00*	$*$ ($*$)/*0.00*	0.17 (0.64)/*0.09*	1.00 (0.68)/*0.09*

TABLE V
INSTANTANEOUS SINGLE-FREQUENCY AMBIGUITY SUCCESS FRACTIONS (RELATIVE FREQUENCIES) AND THE AVERAGE COMPUTATION TIME [SEC] (GIVEN IN BRACKETS) FOR THE HARDWARE-IN-THE-LOOP EXPERIMENT WITH SIMULATED OPEN-PIT USING ELEVATION MASKING; FOR SOME CASES, ONLY A FRACTION OF EPOCHS (GIVEN IN EMPHASIZED TEXT) WERE PROCESSED DUE TO A LACK OF SUFFICIENT SATELLITES FOR POSITIONING (REQUIRES AT LEAST FOUR SATELLITES)

Elevation cut-off [deg]	GPS only Heading	GPS only Elevation	GPS only Bank	Galileo only Heading	Galileo only Elevation	Galileo only Bank	GPS + Galileo Heading	GPS + Galileo Elevation	GPS + Galileo Bank
10	0.07 (0.06)	0.21 (0.21)	0.20 (0.21)	0.05 (0.05)	0.19 (0.20)	0.19 (0.20)	0.04 (0.04)	0.13 (0.14)	0.13 (0.14)
20	0.08 (0.08)	0.31 (0.31)	0.31 (0.32)	0.07 (0.07)	0.28 (0.28)	0.29 (0.29)	0.05 (0.05)	0.19 (0.19)	0.19 (0.19)
30	0.10 (0.10)	0.54 (0.53)	0.53 (0.54)	0.08 (0.08)	0.50 (0.51)	0.53 (0.54)	0.06 (0.06)	0.30 (0.30)	0.30 (0.30)
40	0.12 (0.12)	0.80 (0.80)	0.79 (0.80)	0.12 (0.12)	0.69 (0.71)	0.75 (0.77)	0.09 (0.09)	0.51 (0.52)	0.51 (0.53)
50	0.14 (0.15)	1.27 (1.28)	1.28 (1.32)	0.13 (0.13)	0.82 (0.85)	0.94 (0.99)	0.12 (0.13)	0.97 (0.99)	0.98 (1.02)
60	$*$ ($*$)	$*$ ($*$)	$*$ ($*$)	$*$ ($*$)	$*$ ($*$)	$*$ ($*$)	0.13 (0.13)	1.67 (1.64)	1.68 (1.66)

TABLE VI
EMPIRICAL AND FORMAL (GIVEN IN BRACKETS) ANGULAR STANDARD DEVIATIONS [DEG] FOR HARDWARE-IN-THE-LOOP EXPERIMENT WITH SIMULATED OPEN-PIT USING ELEVATION MASKING

Antenna /Receiver	System (Frequency)	Code σ_{p_0} [cm]	Code a_{p_0}	Code ϵ_{p_0} [deg]	Phase σ_{ϕ_0} [mm]	Phase a_{ϕ_0}	Phase ϵ_{ϕ_0} [deg]
CUT0 & CUTA	GPS (L1)	14	5	20	1	5	20
	Galileo (E1)	8	5	20	1	5	20
CUBB	GPS (L1)	10	10	20	1	25	20
	Galileo (E1)	10	10	20	1	25	20

TABLE VIII
ELEVATION DEPENDENT STOCHASTIC MODEL PARAMETERS (15) FOR CURTIN GNSS STATIONS USED IN THE REAL DATA CAMPAIGNS

ISB	Code ISB [m] (Standard Deviation)	Phase ISB [cycle] (Standard Deviation)
CUTA-CUT0	0.03 (0.001)	0.00 (0.001)
CUBB-CUT0	1.64 (0.001)	-0.46 (0.001)

TABLE IX
DIFFERENTIAL ISB FOR E1-L1 FROM [36]

6 using GPS and GIOVE observations and demonstrate improved performance due to inclusion of GIOVE satellites. For this purpose, we considered data collected on Nov 24, 2011 from 14:06:52 to 20:59:43 (UTC) during which we have long co-visibility of GIOVE-A and GIOVE-B with an elevation cut-off of 10°. Figure 7 shows the satellite visibility (the sky-plot, the number of satellites, and the PDOP values) during the campaign for which both GIOVE-A (PRN E51) and GIOVE-B (PRN E52) satellites were visible (for an elevation cut-off

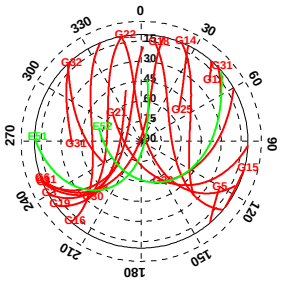

(a) Skyplot (red-GPS and green-Galileo)

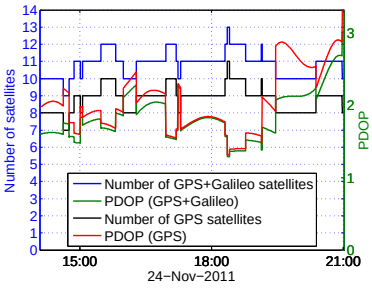

(b) Number of satellites and PDOP

Fig. 7. Visibility of GPS and GIOVE satellites on Dec 19, 2011 for 10° elevation cut-off

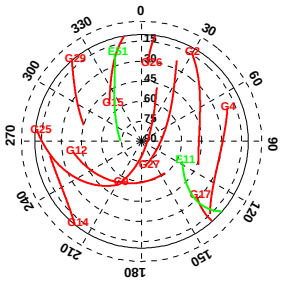

(a) Skyplot (red-GPS and green-Galileo)

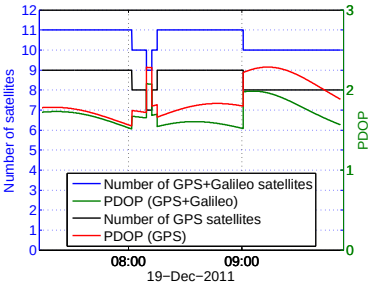

(b) Number of satellites and PDOP

Fig. 8. Satellite visibility of GPS, GIOVE-A, and Galileo-PFM on Dec 19, 2011 for 10° elevation cut-off

angle of 10°). The green curves in the Skyplot correspond to the trajectories of GIOVE satellites. In the following, we discuss the results from single epoch, single-frequency (L1/E1) processing of the data (24772 epochs with 1 sec sampling interval).

Table X reports the instantaneous single-frequency ambiguity success fractions (relative frequencies) and the average computation time (given in brackets) for simulated GPS satellite outages demonstrating the improved success rate performance due to inclusion of GIOVE satellites. Furthermore, the inclusion of GIOVE observations results in a slight improvement of angular accuracy, which is reported in Table XI. Better angular accuracy compared to the hardware-in-the-loop experiment in Table II is due to the use of longer baselines in real data campaign (as shown in Appendix the angular standard deviations are inversely proportional to baseline lengths). The relatively poor bank accuracy is due to the use of a shorter baseline CUT0-CUBB compared to CUT0-CUTA and poorer noise characteristics of CUBB compared to the other two receivers/antennas (cf., Table VIII).

2) GPS/GIOVE-A/Galileo IOV Data: Curtin receivers (Table VII) were among the first to track signals from Galileo-PFM (one of the two Galileo IOV satellites launched on Oct 21, 2011) on Dec 10, 2011. On Dec 19, 2011, Curtin stations for the first time logged navigation data for Galileo-PFM (PRN E11). We considered the data set collected on Dec 19, 2011, from 07:14:00 to 09:52:16 (UTC) during which GIOVE-A and Galileo-PFM were co-visible for an elevation cut-off of 10° (9497 epochs of data). Figure 8 shows the satellite visibility (the sky-plot, the number of satellites, and the PDOP values). The green lines in the Skyplot correspond to the trajectories of GIOVE-A and Galileo-PFM. Since Galileo-PFM was in orbit validation stage, its clock had not been calibrated resulting in large satellite clock error. Due to this large clock error, CUBB did not track E11 continuously. Hence, we considered attitude determination using single baseline formed by CUT0 and CUTA (Table VII). Consequently, we only estimated heading and elevation angles.

Since E11 observations were affected with large satellite clock error and all three clock parameters in the received navigation message were set to zero, we considered an extended model for single point positioning (SPP) by including the satellite clock error for E11 as an additional unknown parameter. Combining the linearized pseudo-range observations from m_G GPS satellites, GIOVE-A, and Galileo-PFM satellites, the system of equations reads:

$$E\left(\begin{bmatrix} \Delta p_{r,1}^{1_G}(t_G) \\ \vdots \\ \Delta p_{r,1}^{m_G}(t_G) \\ \Delta p_{r,1}^{E51}(t_G) \\ \Delta p_{r,1}^{E11}(t_G) \end{bmatrix}\right) = \begin{bmatrix} -e_r^{1_G}(t_G)^T & 1 & 0 & 0 \\ \vdots & \vdots & \vdots & \vdots \\ -e_r^{m_G}(t_G)^T & 1 & 0 & 0 \\ -e_r^{E51}(t_G)^T & 0 & 1 & 0 \\ -e_r^{E11}(t_G)^T & 0 & 1 & 1 \end{bmatrix} \times \begin{bmatrix} \Delta x_r(t_G) \\ c\Delta dt_{r,1}^{G}(t_G) \\ c\Delta dt_{r,1}^{E}(t_G) \\ c\Delta dt_{,1}^{E11}(t_G - \tau_r^{E11}(t_G)) \end{bmatrix} \quad (43)$$

with t_G the observation time in GPS system time, $dt_{r,1}^{G}(t_G)$ the combined receiver clock error and hardware delay, $\Delta p_{r,1}^{s}(t_G) = p_{r,1}^{s}(t_G) - p_{r,1}^{s,0}(t_G)$ the observed-minus-computed observation, $p_{r,1}^{s}(t_G)$ the pseudo-range observation from satellite s at frequency $L1$ or $E1$, $e_r^s(t_G) = \frac{(x^s(t-\tau_r^s(t_G)) - x_r(t_G))}{\rho_r^s(t_G - \tau_r^s(t_G), t_G)}$ the unit vector from receiver at time t_G to satellite at time $t_G -$

GPS only			GPS+GIOVE		
# Sat (PDOP)	LAMBDA	MC-LAMBDA	# Sat (PDOP)	LAMBDA	MC-LAMBDA
4 (9.41)	0.00 (0.12)	0.12 (0.58)	6 (6.74)	0.02 (0.14)	0.94 (0.26)
5 (5.50)	0.00 (0.11)	0.81 (0.51)	7 (4.33)	0.33 (0.14)	0.99 (0.20)
6 (3.59)	0.03 (0.12)	0.98 (0.34)	8 (3.22)	0.66 (0.15)	**1.00** (0.20)
7 (2.46)	0.19 (0.12)	0.99 (0.17)	9 (2.22)	0.81 (0.15)	**1.00** (0.19)
8 (2.17)	0.52 (0.13)	1.00 (0.19)	10 (1.97)	0.93 (0.16)	1.00 (0.19)
9 (2.07)	0.72 (0.13)	1.00 (0.17)	11 (1.87)	0.97 (0.18)	1.00 (0.21)
10 (2.05)	0.77 (0.13)	1.00 (0.18)	12 (1.85)	0.97 (0.18)	1.00 (0.21)

TABLE X
INSTANTANEOUS SINGLE-FREQUENCY AMBIGUITY SUCCESS FRACTIONS (RELATIVE FREQUENCIES) AND THE AVERAGE COMPUTATION TIME [SEC] (GIVEN IN BRACKETS) FOR GPS ONLY AND GPS+GIOVE; '# SAT' REFERS TO NUMBER OF SATELLITES

GPS only				GPS+GIOVE			
# Sat	Heading	Elevation	Bank	# Sat	Heading	Elevation	Bank
4	0.04 (0.04)	0.10 (0.09)	0.26 (0.29)	6	0.02 (0.02)	0.05 (0.04)	0.20 (0.19)
5	0.02 (0.02)	0.06 (0.06)	0.18 (0.23)	7	0.02 (0.02)	0.05 (0.04)	0.17 (0.17)
6	0.02 (0.02)	0.05 (0.04)	0.15 (0.17)	8	0.02 (0.01)	0.04 (0.03)	0.15 (0.15)
7	0.02 (0.01)	0.04 (0.03)	0.14 (0.16)	9	0.01 (0.01)	0.04 (0.03)	0.14 (0.14)
8	0.01 (0.01)	0.04 (0.03)	0.14 (0.14)	10	0.01 (0.01)	0.03 (0.03)	0.14 (0.13)
9	0.01 (0.01)	0.04 (0.03)	0.14 (0.13)	11	0.01 (0.01)	0.03 (0.03)	0.14 (0.12)
10	0.01 (0.01)	0.04 (0.03)	0.14 (0.13)	12	0.01 (0.01)	0.03 (0.03)	0.14 (0.12)

TABLE XI
EMPIRICAL AND FORMAL (GIVEN IN BRACKETS) ANGULAR STANDARD DEVIATIONS [DEG] FOR GPS ONLY AND GPS+GIOVE; '# SAT' REFERS TO NUMBER OF SATELLITES

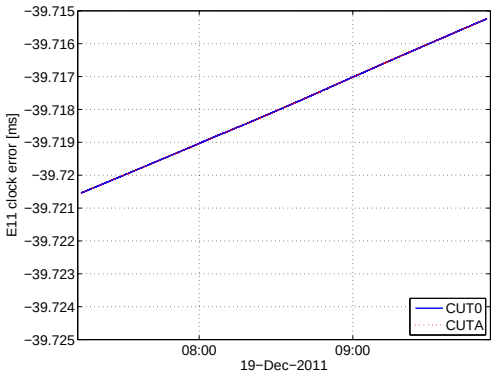

Fig. 9. Estimates of E11 clock error based on SPP solutions of CUT0 and CUTA using extended model (43)

	Clock bias (a_0) [10^{-2} sec]	Clock drift (a_1) [10^{-10} sec/sec]	Clock drift rate (a_2) [10^{-15} sec/sec^2]
CUT0	−3.9733	4.2479	2.1900
CUTA	−3.9733	4.2924	2.1197

TABLE XII
E11 CLOCK ERROR BASED ON SINGLE POINT POSITIONING USING THE EXTENDED MODEL IN (43)

GPS only			GPS + GIOVE-A + Galileo-PFM		
# Sat	Heading	Elevation	# Sat	Heading	Elevation
4	0.03 (0.03)	0.07 (0.06)	6	0.02 (0.02)	0.05 (0.05)
5	0.02 (0.02)	0.05 (0.04)	7	0.02 (0.01)	0.04 (0.03)
6	0.02 (0.02)	0.05 (0.04)	8	0.02 (0.01)	0.04 (0.03)
7	0.02 (0.01)	0.04 (0.03)	9	0.01 (0.01)	0.03 (0.03)
8	0.02 (0.01)	0.04 (0.03)	10	0.01 (0.01)	0.03 (0.03)
9	0.01 (0.01)	0.03 (0.03)	11	0.01 (0.01)	0.03 (0.03)
10	0.01 (0.01)	0.03 (0.03)	12	0.01 (0.01)	0.03 (0.03)

TABLE XIV
EMPIRICAL AND FORMAL (GIVEN IN BRACKETS) ANGULAR STANDARD DEVIATIONS [DEG] FOR GPS ONLY AND GPS + GIOVE-A + GALILEO-PFM; '# SAT' REFERS TO NUMBER OF SATELLITES

$\tau_r^s(t_G)$, $\tau_r^s(t_G)$ the signal travel time, and $\rho_r^s(t_G - \tau_r^s(t_G), t_G)$ the topocentric distance between receiver at time t_G to satellite at time $t_G - \tau_r^s(t_G)$. Prefix Δ in the right-hand side of the above equation refers to the correction in the iterative least-squares estimation.

The estimated E11 clock error is shown in Figure 9. Using satellite clock error model $a_0 + a_1\delta t + a_2\delta t^2$, where δt is the difference between observation time and signal transmission, the model parameters for E11 satellite clock error, a_0, a_1, and a_2, are estimated. As reported in Table XII it indicates a large clock bias. Note that due to the additional parameter to be estimated in (43), Galileo code observations do not contribute to absolute positioning. However, this clock error gets eliminated in double differencing. Hence, Galileo observations do contribute to relative positioning. In the following, we discuss the results of single epoch, single-frequency (L1/E1) processing of this data (9497 epochs at a rate of 1 Hz).

Table XIII reports the instantaneous single-frequency ambiguity success fractions (relative frequencies) and the average computation time (given in brackets) for simulated GPS satellite outages. Similar to GPS-GIOVE processing in Section III-B1, it demonstrates the improved success rate performance due to inclusion of GIOVE-A and Galileo-PFM satellites. Also the inclusion of GIOVE-A and Galileo-PFM observations results in a slight improvement of angular accuracy, which is reported in Table XIV. As we have the same (first) baseline in this analyses and that in Section III-B1, angular accuracies in Table XIV are well in line with that in Table XI.

IV. SUMMARY AND CONCLUSIONS

In this contribution a combined GPS+Galileo performance and robustness analysis was carried out for instantaneous

GPS only			GPS + GIOVE-A + Galileo-PFM		
# Sat (PDOP)	LAMBDA	MC-LAMBDA	# Sat (PDOP)	LAMBDA	MC-LAMBDA
4 (9.98)	0.00 (0.07)	0.33 (0.08)	6 (6.32)	0.47 (0.09)	0.97 (0.09)
5 (3.55)	0.05 (0.07)	0.77 (0.07)	7 (3.11)	0.82 (0.09)	**1.00** (0.09)
6 (2.70)	0.34 (0.07)	0.95 (0.07)	8 (2.34)	0.98 (0.09)	**1.00** (0.09)
7 (2.13)	0.77 (0.07)	1.00 (0.07)	9 (1.93)	0.99 (0.09)	1.00 (0.09)
8 (2.01)	0.96 (0.08)	1.00 (0.08)	10 (1.81)	**1.00** (0.10)	1.00 (0.10)
9 (1.89)	0.99 (0.08)	1.00 (0.08)	11 (1.70)	**1.00** (0.10)	1.00 (0.11)
10 (1.89)	0.99 (0.08)	1.00 (0.08)	12 (1.70)	**1.00** (0.10)	1.00 (0.11)

TABLE XIII
INSTANTANEOUS SINGLE-FREQUENCY AMBIGUITY SUCCESS FRACTIONS (RELATIVE FREQUENCIES) AND THE AVERAGE COMPUTATION TIME [SEC] (GIVEN IN BRACKETS) FOR GPS ONLY AND GPS+GIOVE-A+GALILEO-PFM; '# SAT' REFERS TO NUMBER OF SATELLITES

single-frequency attitude determination. Improved availability and angular accuracy were demonstrated using data from a hardware-in-the-loop experiment as well as from real data campaigns. We considered various satellite deprived environments (satellite outage, urban canyon, and open-pit) to study the robustness of the GPS/Galileo-based attitude solutions. In comparing the performances of LAMBDA and MC-LAMBDA, we also studied the impact of using the known antenna-geometry on ambiguity resolution.

It was shown, using simulated satellite outages, that instantaneous single-frequency ambiguity resolution using the MC-LAMBDA method is possible with as few as six satellites from GPS and/or Galileo constellations. It was also shown for satellite masking effect of the urban canyon environment, that combined GPS/Galileo processing still enables instantaneous attitude determination in case buildings are 9 meter tall, 17 meter wide and symmetrically placed on both sides of a ten-meter wide urban road. And it was shown that the use of a combined GPS/Galileo constellation enables instantaneous open-pit attitude determination with elevation masking as large as 40 degrees, while one can only go up to 20 degree elevation masking with a single system.

Further to the hardware-in-the-loop experiment, we used two real data sets involving Galileo experimental satellites to validate the above findings. Processing of the first real data set consisting of data from two GIOVE satellites confirmed the significant advantages of using a combined system. Finally, we demonstrated that the Galileo-PFM satellite, which is in the early stage of testing phase, has already contributed to attitude solution availability in the case of a number of GPS satellite outages.

Important for future research in the field of GNSS attitude determination is the further development of a probabilistic framework, similar to the one already available for the standard mixed-integer GNSS model [47], [48]. Such theoretical framework would allow for the development of the appropriate probability density functions and test statistics for the constrained GNSS attitude model.

APPENDIX

In this section we derive the formal variance-covariance matrix of attitude angular estimates $\xi\left(\check{Z}\right)$ in (38). The linearized version of (38) reads

$$\begin{array}{rcl} \mathrm{E}\left(\mathrm{vec}\left(\Delta\hat{R}(\check{Z})\right)\right) & = & J_{R,\xi}(\xi_0)\Delta\xi \\ \mathrm{D}\left(\mathrm{vec}\left(\hat{R}(\check{Z})\right)\right) & = & Q_{\hat{R}(Z)\hat{R}(Z)} \end{array} \tag{44}$$

where $\Delta\hat{R}(\check{Z}) = \hat{R}(\check{Z}) - R(\xi_0)$, $\Delta\xi = \xi - \xi_0$, and $J_{R,\xi}(\xi_0)$ is the Jacobian matrix evaluated at intermediate estimate ξ_0 from the iterative least squares estimation and given as

$$J_{R,\xi} = \left[J_1^T \dots J_q^T\right]^T \tag{45}$$

with

$$\text{if } q=1 \quad J_1 = \begin{bmatrix} -s_\phi c_\theta & -c_\phi s_\theta \\ c_\phi c_\theta & -s_\phi s_\theta \\ 0 & -c_\theta \end{bmatrix}$$

$$\text{else} \quad J_1 = \begin{bmatrix} -s_\phi c_\theta & -c_\phi s_\theta & 0 \\ c_\phi c_\theta & -s_\phi s_\theta & 0 \\ 0 & -c_\theta & 0 \end{bmatrix}$$

and

$$J_2 = \begin{bmatrix} -s_\phi s_\theta s_\psi - c_\phi c_\psi & c_\phi c_\theta s_\psi & c_\phi s_\theta c_\psi + s_\phi s_\psi \\ c_\phi s_\theta s_\psi - s_\phi c_\psi & s_\phi c_\theta s_\psi & s_\phi s_\theta c_\psi - c_\phi s_\psi \\ 0 & -s_\theta s_\psi & c_\theta c_\psi \end{bmatrix}$$

$$J_3 = \begin{bmatrix} -s_\phi s_\theta c_\psi + c_\phi s_\psi & c_\phi c_\theta c_\psi & -c_\phi s_\theta s_\psi + s_\phi c_\psi \\ c_\phi s_\theta c_\psi + s_\phi s_\psi & s_\phi c_\theta c_\psi & -s_\phi s_\theta s_\psi - c_\phi c_\psi \\ 0 & -s_\theta c_\psi & -c_\theta s_\psi \end{bmatrix}$$

The variance-covariance matrix of attitude angular estimates at least-squares solution $\hat{\xi}$ is given as

$$Q_{\xi\xi} \approx \left(J_{R,\xi}(\hat{\xi})^T Q^{-1}_{\hat{R}(Z)\hat{R}(Z)} J_{R,\xi}(\hat{\xi})\right)^{-1} \tag{46}$$

Using (33), the variance-covariance matrix of attitude angles can be written as

$$Q_{\xi\xi} = \left(J_{R,\xi}(\hat{\xi})^T \left(\mathcal{P}^{-1} \otimes \mathcal{S}^{-1}\right) J_{R,\xi}(\hat{\xi})\right)^{-1} \tag{47}$$

where $\mathcal{P} = \left(B_0 P^{-1} B_0^T\right)^{-1}$ and $\mathcal{S} = \left(G^T Q_{yy}^{-1} G\right)^{-1}$. Hence, the angular estimation accuracy depends on antenna geometry ($\mathcal{P}$), attitude angles, receiver-satellite geometry (G), and observation variance-covariance matrix (Q_{yy}). Using (45), the above can be written as

$$Q_{\xi\xi} = \left(\sum_{i=1}^{q}\sum_{j=1}^{q} \mathcal{P}_{ij}^{-} J_i^T \mathcal{S}^{-1} J_j\right)^{-1} \tag{48}$$

where $\mathcal{P}_{ij}^{-}$ is the i,j element of $\mathcal{P}^{-1}$. If we increase the lengths of the baselines (such that $B_0^l = lB_0$) then the variance matrix reads

$$Q_{\xi\xi}^l = \frac{1}{l^2}\left(\sum_{i=1}^{q}\sum_{j=1}^{q}\mathcal{P}_{ij}^{-}J_i^T\mathcal{S}^{-1}J_j\right)^{-1} \quad (49)$$

$$= \frac{1}{l^2}Q_{\xi\xi} \quad (50)$$

Hence, the angular standard deviation is inversely proportional to baseline length.

ACKNOWLEDGMENT

The second author P.J.G. Teunissen is the recipient of an Australian Research Council Federation Fellowship (project number FF0883188). This work is supported by the Australian Space Research Program GARADA project on SAR Formation Flying. All these supports are gratefully acknowledged.

REFERENCES

[1] C. Cohen, "Attitude determination using GPS," Ph.D. dissertation, Stanford University, 1992.

[2] G. Lu, "Development of a GPS multi-antenna system for attitude determination," Ph.D. dissertation, Department of Geomatics Engineering, University of Calgary, 1995.

[3] C.-H. Tu, K. Tu, F.-R. Chang, and L.-S. Wang, "GPS compass: A novel navigation equipment," *Aerospace and Electronic Systems, IEEE Transactions on*, vol. 33, no. 3, pp. 1063 –1068, July 1997.

[4] J. L. Crassidis and F. L. Markley, "New algorithm for attitude determination using Global Positioning System signals," *Journal of Guidance, Control, and Dynamics*, vol. 20, no. 5, pp. 891–896, September-October 1997.

[5] P. Montgomery, I. Y. Bar-Itzhack, and J. Garrick, "Algorithm for attitude determination using GPS," in *Proceedings Guidance, Navigation and Control Conference*, 1999.

[6] H. M. Peng, F. R. Chang, and L. S. Wang, "Attitude determination using GPS carrier phase and compass data," in *Proceedings of ION NTM 99.*, 1999.

[7] Y. Li, K. Zhang, C. Roberts, and M. Murata, "On-the-fly GPS-based attitude determination using single- and double-differenced carrier phase measurements," *GPS Solutions*, vol. 8, no. 2, pp. 93–102, 2004.

[8] D. Lin, L. Voon, and N. Nagarajan, "Real-time attitude determination for microsatellite by LAMBDA method combined with Kalman filtering," in *22 nd AIAA International Communications Satellite Systems Conference and Exhibit 2004*, Monterey, California, USA, 2004.

[9] J. Madsen and E. G. Lightsey, "Robust spacecraft attitude determination using global positioning system receivers," *Journal of Spacecraft and Rockets*, vol. 41, no. 4, pp. 635–643, July-August 2004.

[10] M. L. Psiaki, "Batch algorithm for global-positioning-system attitude determination and integer ambiguity resolution," *Journal od Guidance, Control, and Dynamics*, vol. 29, no. 5, pp. 1070–1079, September-October 2006.

[11] C. Hide, J. Pinchin, and D. Park, "Development of a low cost multiple GPS antenna attitude system," in *Proceedings of ION GNSS 20th International Technical Meeting of the Satellite Division*, Fort Worth, TX, September 2007.

[12] D. Aloi and O. Korniyenko, "Comparative performance analysis of a Kalman filter and a modified double exponential filter for GPS-Only position estimation of automotive platforms in an urban-canyon environment," *Vehicular Technology, IEEE Transactions on*, vol. 56, no. 5, pp. 2880 –2892, sept. 2007.

[13] L. Johnson and F. van Diggelen, "Advantages of a combined GPS+GLONASS precision sensor for machine control applications in open pit mining," in *Position Location and Navigation Symposium, IEEE 1998*, apr 1998, pp. 549 –554.

[14] P. J. G. Teunissen, "The least-squares ambiguity decorrelation adjustment: a method for fast GPS integer ambiguity estimation," *Journal of Geodesy*, vol. 70, pp. 65–82, 1995.

[15] F. Boon and B. Ambrosius, "Results of real-time applications of the LAMBDA method in GPS based aircraft landings," in *Proceedings KIS97*, 1997, pp. 339–345.

[16] D. Cox, "Integration of LAMBDA ambiguity resolution with Kalman filter for relative navigation of spacecraft," in *Institute of Navigation, Annual Meeting, 55 th, Cambridge, MA*, 1999, pp. 739–745.

[17] S. Ji, W. Chen, C. Zhao, X. Ding, and Y. Chen, "Single epoch ambiguity resolution for Galileo with the CAR and LAMBDA methods," *GPS Solutions*, vol. 11, pp. 259–268, 2007.

[18] S. Huang, J. Wang, X. Wang, and J. Chen, "The application of the LAMBDA method in the estimation of the GPS slant wet vapour," *Acta Astronomica Sinica*, vol. 50, pp. 60–68, 2009.

[19] R. Kroes, O. Montenbruck, W. Bertiger, and P. Visser, "Precise GRACE baseline determination using GPS," *GPS Solutions*, vol. 9, pp. 21–31, 2005.

[20] P. J. G. Teunissen, "The affine constrained GNSS attitude model and its multivariate integer least-squares solution," *Journal of Geodesy*, vol. 86, no. 7, pp. 547–563, 2012.

[21] ——, "An optimality property of the integer least-squares estimator," *Journal of Geodesy*, vol. 73, pp. 587–593, 1999.

[22] P. J. G. Teunissen, P. De Jonge, and C. Tiberius, "Performance of the LAMBDA method for fast GPS ambiguity resolution," *Navigation*, vol. 44, no. 3, pp. 373–383, 1997.

[23] S. Verhagen and P. J. G. Teunissen, "New global navigation satellite system ambiguity resolution method compared to existing approaches," *Journal of Guidance, Control, and Dynamics*, vol. 29, no. 4, pp. 981–991, 2006.

[24] C. Park and P. J. G. Teunissen, "A new carrier phase ambiguity estimation for GNSS attitude determination systems," in *Proceedings of International Symposium on GPS/GNSS*, Tokyo, Japan, 2003, pp. 283–290.

[25] P. J. G. Teunissen, "A general multivariate formulation of the multi-antenna GNSS attitude determination problem," *Artificial Satellites*, vol. 42, no. 2, pp. 97–111, 2007.

[26] P. J. Buist, "The baseline constrained LAMBDA method for single epoch, single frequency attitude determination applications," in *Proceedings of the 20th International Technical Meeting of the Satellite Division of The Institute of Navigation (ION GNSS 2007)*, Fort Worth, TX, USA, 2007, pp. 2962 – 2973.

[27] C. Park and P. J. G. Teunissen, "Integer least squares with quadratic equality constraints and its application to GNSS attitude determination systems," *International Journal of Control, Automation, and Systems*, vol. 7, no. 4, pp. 566–576, 2009.

[28] G. Giorgi, P. J. G. Teunissen, and P. J. Buist, "A search and shrink approach for the baseline constrained LAMBDA method: Experimental results," in *Proceedings of International Symposium on GPS/GNSS*, A. Yasuda, Ed., Tokyo University of Marine Science and Technology, 2008, pp. 797 – 806.

[29] G. Giorgi and P. Buist, "Single-epoch, single-frequency, standalone full attitude determination: experimental results," in *Proceedings of the 4th ESA Workshop on Satellite Navigation User Equipment Technologies, NAVITEC*, ESA-ESTEC, The Netherlands, 2008, p. 8.

[30] P. J. G. Teunissen, G. Giorgi, and P. J. Buist, "Testing of a new single-frequency GNSS carrier phase attitude determination method: Land, ship and aircraft experiments," *GPS Solutions*, vol. 15, no. 1, pp. 15–28, 2011.

[31] G. Giorgi, P. J. G. Teunissen, S. Verhagen, and P. J. Buist, "Instantaneous ambiguity resolution in Global-Navigation-Satellite-System-based attitude determination applications: A multivariate constrained approach," *Journal of Guidance, Control, and Dynamics*, vol. 35, no. 1, pp. 51–67, 2012.

[32] N. Nadarajah, P. J. G. Teunissen, and G. Giorgi, "GNSS attitude determination for remote sensing: On the bounding of the multivariate ambiguity objective function," in *Proceedings of International Association of Geodesy Symposia (IAGS-2011)*, Melbourne, Australia, 28 June - 7 July 2011.

[33] S. Verhagen and P. Joosten, "Algorithms for design computations for integrated GPS-Galileo," in *Proceedings of the European Navigation Conference (ENC-GNSS 2003)*, 2003.

[34] O. Julien, P. Alves, M. E. Cannon, and W. Zhang, "A tightly coupled GPS/GALILEO combination for improved ambiguity resolution," in *Proceedings of the European Navigation Conference (ENC-GNSS03)*, 2003, pp. 1–14.

[35] O. Julien, M. Cannon, P. Alves, and G. Lachapelle, "Triple frequency ambiguity resolution using GPS/Galileo," *European Journal of Navigation*, vol. 2, no. 2, pp. 51–57, 2004.

[36] D. Odijk, P. J. G. Teunissen, and L. Huisman, "First results of mixed GPS+GIOVE single-frequency RTK in Australia," *Journal of Spatial Sciences*, vol. 57, no. 1, pp. 3–18, June 2012, (to appear).
[37] P. J. G. Teunissen and A. Kleusberg, *GPS for Geodesy*, 2nd ed. Springer, 1998.
[38] H.-J. Euler and C. Goad, "On optimal filtering of GPS dual frequency observations without using orbit information," *Journal of Geodesy*, vol. 65, pp. 130–143, 1991.
[39] D. A. Harville, *Matrix Algebra From A Statisticians Perspective*. New York: Springer, 1997.
[40] J. R. Magnus and H. Neudecker, *Matrix differential calculus with applications in statistics and econometrics*. New York: Wiley, 1995.
[41] P. J. G. Teunissen, "A-PPP: Array-aided precise point positioning with global navigation satellite systems," *IEEE Transactions on Signal Processing*, vol. 60, no. 6, pp. 2870 –2881, June 2012.
[42] M. Tsakiri, M. Stewart, T. Forward, D. Sandison, and J. Walker, "Urban fleet monitoring with GPS and GLONASS," *The Journal of Navigation*, vol. 51, no. 03, pp. 382–393, 1998.
[43] I. Ballester-Grpide, E. Herriz-Monseco, A. J.-M. andMiguel M. Romay-Merino, and T. W. Beech, "Future GNSS constellation performances inside urban environments," in *Proceedings of the 13th International Technical Meeting of the Satellite Division of The Institute of Navigation (ION GPS 2000)*, Salt Lake City, UT, September 2000, pp. 2436–2445.
[44] S. Ji, W. Chen, X. Ding, Y. Chen, C. Zhao, and C. Hu, "Potential benefits of GPS/GLONASS/Galileo integration in an urban canyon - Hong Kong," *The Journal of Navigation*, vol. 63, no. 04, pp. 681–693, 2010.
[45] E. Bertran and J. Delgado-Penin, "On the use of GPS receivers in railway environments," *Vehicular Technology, IEEE Transactions on*, vol. 53, no. 5, pp. 1452 – 1460, sept. 2004.
[46] G. Giorgi, "GNSS carrier phase-based attitude determination estimation and applications," Ph.D. dissertation, Delft University of Technology, December 2011.
[47] P. J. G. Teunissen, "The parameter distributions of the integer GPS model," *Journal of Geodesy*, vol. 76, no. 1, pp. 41–49, 2002.
[48] S. Verhagen and P. J. G. Teunissen, "On the probability density function of the ambiguity residuals," *GPS Solutions*, vol. 10, no. 1, pp. 21–28, 2006.

Nandakumaran Nadarajah received the B.Sc.Eng. degree in electrical and electronic engineering from University of Peradeniya, Peradeniya, Sri Lanka, in 2001, and the M.A.Sc and Ph.D. degrees in electrical and computer engineering from McMaster University, Canada, in 2005 and 2009, respectively. From 2002 to 2003 he was an Assistant Lecturer at Department of Electrical and Electronic Engineering, University of Peradeniya, Sri Lanka. From 2003 to 2009 he was a graduate student/research assistant at Department of Electrical and Computer Engineering, McMaster University, Canada. Currently, he is working as a research fellow at GNSS Research Centre, Curtin University. His research interests are in attitude determination, relative navigation, signal processing, and target tracking.

Peter Teunissen is a Federation Fellow of the Australian Research Council (ARC), Professor of Geodesy and Navigation, Science Director of the Cooperative Research Centre for Spatial Information, and Head of CUT's Global Navigation Satellite System (GNSS) Research Centre. His current research focus is on modelling next-generation GNSS for relative navigation and attitude determination in space and air.

Noor Raziq received his B.Sc. in civil engineering with honours from University of Engineering and Technology, Peshawar, KPK, Pakistan in 1999 and Ph.D. in Geomatics engineering from the University of Melbourne, Australia, in 2009. He has been working in various engineering roles in civil engineering and GPS from 1999 to 2011. Currently, Noor is working as a GNSS research fellow at GNSS Research Centre, Department of Spatial Sciences, Curtin University. His research interest are high precision GNSS and engineering applications of GNSS.